applied sciences

MDPI

Article

Circulating Current Reduction in MMC-HVDC System Using Average Model

Kamran Hafeez [1,*], Shahid A. Khan [1], Alex Van den Bossche [2] and Qadeer Ul Hasan [1]

[1] Department of Electrical Engineering, COMSATS University, Park Road, Islamabad 44000, Pakistan; shahidk@comsats.edu.pk (S.A.K.); qadeer.hasan@comsats.edu.pk (Q.U.H.)

[2] Department of Electrical Engineering, Metals, Mechanical Constructions and Systems, Ghent University, Technology park Zwijnaarde 131, B-9052 Zwijnaarde, Gent, Belgium; alex.vandenbossche@ugent.be

* Correspondence: kamran.hafeez@comsats.edu.pk; Tel.: +92-314-90-37950

Received: 6 March 2019; Accepted: 28 March 2019; Published: 1 April 2019

Abstract: Modular multilevel converters (MMCs) are quickly emerging as a suitable technology for a voltage-source converter-based high-voltage direct-current (VSC-HVDC) transmission systems due to its numerous advantages as reported in literature. However, for a large DC-network, MMCs require large numbers of sub-modules (SMs) and switches, which makes its modeling very challenging and computationally complex using electromagnetic transient (EMT) programs. Average Value Model (AVM) provides a relatively better solution to model MMCs by combining cells as an arm equivalent circuit. Circulating current is an important issue related to the performance and stability of MMCs. Due to circulating currents, power loss in a converter increases as root mean square (RMS) values of the arm current increases. The traditional method for inserting SMs in each arm is based on direct modulation, which does not compensate for the arm voltage oscillations, and generates circulating current in each leg of a three-phase MMC. This paper presents a new method for reducing the circulating current by adding 2nd and 4th harmonics in the upper and lower arm currents of an MMC. Less capacitor energy variations are obtained by the proposed method compared to traditional direct modulation methods. The proposed method is tested on a common symmetrical monopole (point-to-point) MMC-HVDC system using vector current control strategy in PSCAD/EMTDC software. Analytical and simulation results show the effectiveness of the new method in minimizing the circulating current and arm voltage oscillation reductions as compared to the direct modulation approach.

Keywords: average-value model; electromagnetic-transient (EMT) program; HVDC transmission; modular multilevel converter; voltage-source converter (VSC)

1. Introduction

Among the voltage-source-power converters (VSCs), the modular multilevel converter (MMC) is emerging as a potential candidate for high voltage DC transmission systems [1]. It offers several advantages, such as the absence of large power supplies at each module, lower harmonics, less switching losses, modular structure, and scalable output voltage [2]. However, the working principle of MMC is different from other VSC (two levels and three levels converters) as it is based on the physical insertion and bypassing of its sub-modules (SMs) in a discrete pattern, making its control mechanism and overall structure complex [3]. Electromagnetic Transients Program (EMTP)-type programs, like PSCAD/EMTDC, are normally applied to study the dynamics of such a complex power converter system [4].

MMCs introduce a big challenge for its modeling in electromagnetic transient (EMT) simulation programs due to the increased number of switches and modules. The complete details about the

different versions of MMC models are available in Reference [5]. To model switch behavior, the total number of nodes in a network representing an admittance matrix must be re-triangulated during switching operation [6].

In detailed models (DMs), thousands of semiconductor switches are accurately modeled to study the dynamics of MMC-based high-voltage direct-current (HVDC) systems, but computational burden becomes very high. The simplified models, or average-value models (AVMs), have been used to overcome this problem, but they did not reflect the actual dynamics, as switch functions are simplified using controlled voltage and current sources [7]. AVMs also neglect switching details and make system dynamics approximate, leading to fast computation speeds [8].To study slow dynamics of large systems like DC grids, the AVM-based models are more computer-efficient than detailed MMC models [9]. Details of the different types of models are already explained in Reference [10] and can be classified as (1) detailed model; (2) arm equivalent circuit (The venin equivalent) model; (3) arm switch model; and (4) average model. A comprehensive review of these models for EMT-type studies is reported in Reference [11], focusing on transient conditions. Different methods of MMC control and its application are highlighted in Reference [12] without considering modeling techniques. Implementing detailed models is unrealistic for EMT-type computer simulation programs due to the computational complexity. The arm/the venin's equivalent model is computer-efficient but less accurate. The arm switch and average models are computer-efficient but cannot be used for the balancing control of sub-module capacitors (SMs). The continuous model of MMC is developed in Reference [13], which is based on the equivalent branch model of an arm comprising resistance, inductance, and an ideal voltage source. The stability analysis framework of continuous model is discussed in Reference [14]. In Reference [15], interaction between arm current and capacitor voltages are documented using the direct modulation approach. The drawback of this approach is the presence of a circulating current inside the arm current, since it assumes average SM capacitor voltage, which results in arm voltage oscillations and circulating current generation inside MMCs. A compensated modulation technique is used to eliminate the circulating current by considering the voltage ripple estimation that will compensate arm voltage oscillations based on the measurement of amplitude and phase of the output current [16]. In Reference [17], the analytical expressions for circular current interaction with arm voltage and arm current of MMCs was developed. The grid-side AC current and circulating current is controlled separately using proportional resonant (PR)and proportional (P) or gain controllers, which ultimately minimizes SM capacitance fluctuations as proposed in Reference [18]. The important tasks for the operation of MMCs is to control output voltages and currents while keeping balance between SM capacitor voltages and the control of circulating currents. The circulating current can influence the proper functioning of converters by increasing its overall ratings and power losses. The advantages of circulating current elimination or minimization is already discussed in References [19,20]. The double-carrier phase disposition pulse width modulation (PWM) technique is discussed in Reference [21], which eliminates the AC component of the circulating current using a high pass filter and differential current control using a proportional integral (PI) controller to minimize power losses at the cost of capacitor voltage ripple. A plug-in repetitive controller was implemented in Reference [22], which also reduces circulating current by eliminating lower order harmonics. To regulate AC side currents and eliminate circulating currents from arm currents, two separate controllers are normally adopted in MMC-HVDC systems; however, three separate current controllers are proposed in Reference [23] to control arm currents without implementing an AC side controller. To reduce converter losses, higher order harmonics can be eliminated from the circulating current but increases voltage ripples in SM capacitors; whereas injecting harmonics in circulating currents reduces cell capacitance, as proposed in Reference [24], but increases RMS values of arm currents. In Reference [25], SM capacitor voltage ripple is minimized by adding higher order harmonics inside the circulating current at the cost of increasing the RMS value of arm currents. It is evident that existing circulating current control methods can be divided in two groups: (1) elimination of higher order harmonics, which in turn increases SM capacitor voltage ripples but reduce the RMS value of

arm currents; and (2) injecting higher order harmonics inside circulating currents reduces the capacitor voltage ripple but increases the RMS value of the arm current unless circulating current injection ratio is calculated accurately, further increasing the burden on the system [26].

The objective of this research work is to implement an MMC-HVDC system based on the average model developed in References [13,14]. It is a nonlinear average model, which can capture circulating current phenomena by inserting SMs in a continuous manner. It can also be used as a bench mark circuit [27]; however, unlike Reference [14], which implements a circulating current suppression controller to reduce differential current inside MMC, a new method is proposed for reducing the circulating current. In this proposed method, a new technique is used for the addition of higher order harmonics in the upper and lower arm currents in each leg of an MMC; which will lead to a decreased inflow of excessive negative currents in a period. A reduced capacitor energy variation is obtained as arm voltage oscillations is the sum of all the capacitor voltages, which ultimately reduces the flow of the circulating current in each leg of a three-phase MMC. Furthermore, it will not affect the input and output current waveforms of the MMCs. The direct and proposed methods were tested on a common MMC-HVDC system using the PSCAD simulation program based on nonlinear AVM models.

To the best of the author's knowledge, the key contributions are summarized as follows:

(1) The existing direct modulation technique generates sinusoidal arm currents that cause variations in capacitor energy, leading to capacitor voltage fluctuations. In the past, different approaches were adopted to minimize capacitor voltage fluctuations.
(2) In some papers, harmonics were injected inside the circulating current, which reduced voltage fluctuations but led to increases in RMS values of arm currents, causing excessive power loss.
(3) In another approach, differential current controllers were used to control capacitor voltage fluctuations, which increases the hardware burden on system as well as additional controller specific adjustments.
(4) However, in this research work, a new method is proposed to minimize capacitor energy variations by injecting even order harmonics to the upper and lower arm currents, which restricts excessive negative currents in each arm of the MMC, leading to the presence of DC current components. This also results in the reduction of circulating currents and RMS values of the arm current inside each leg of the MMC, which is evident from analytical and simulation results reported in this paper.
(5) The proposed method is implemented on a point-to-point MMC-HVDC test system based on a non-linear AVM model using the vector current control method.

Section 2 describes the MMC-HVDC system topology and its operational principle, and Section 3 explains the control system design of the MMC-HVDC system. The development of the AVM model is presented in Section 4. In Section 5, voltage references are derived based on direct and proposed direct modulation methods along with the flow chart of the proposed method. Section 6 presents analytical and simulations results by comparing capacitor energy variations using the traditional direct modulation method and the effect of 2nd and 4th harmonics on capacitor energy variations, which validates the accuracy of the proposed method. Finally, conclusions are drawn in Section 7.

2. MMC-HVDC System Structure

Figure 1a,b shows the single line diagram of the MMC-HVDC system and circuit diagram of a three-phase MMC converter (double-star configuration) as proposed in Reference [28], respectively. The HVDC system includes two MMCs working as a rectifier and inverter connected at each side of an AC system through a three-phase transformer. The sub-modules (SMs), or cells, are used to develop a half-bridge circuit. Each cell is made of a capacitor and two Insulated-gate bipolar transistors (IGBTs) switches (T_1, T2) connected in series. The cell output voltage (V_{sm}) is equal to the capacitor voltage (T_1 on state) or zero (T_1 off state) and is regulated by the controller. The switching states of the cells are controlled so that at any instant, n cells out of $2n$ cells are on (n_{up} in the upper arm and $n_{low} = n - n_{up}$

in the lower arm) in each phase. Each arm consists of n series of connected cells and an inductor L_{arm} in series, which is used to limit the fault current. Each leg comprises two arms, which can be represented as a controllable voltage source, i.e., V_{up} and V_{low}. The converter terminal voltage at the AC side in phase a can be expressed as follows:

$$V_{C(a)} = \frac{n_{low} - n_{up}}{2n} V_{dc} \tag{1}$$

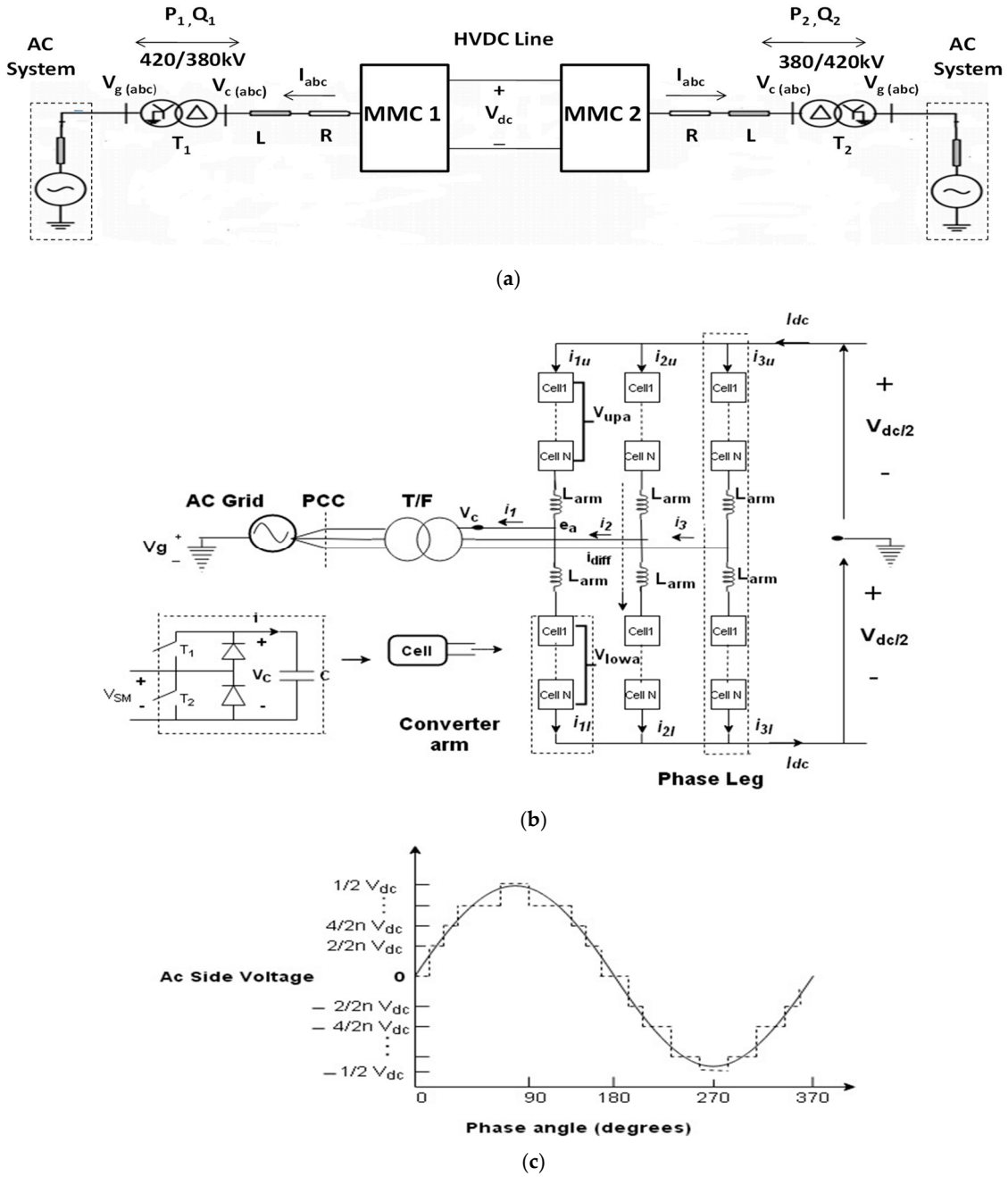

Figure 1. Modular multilevel converter-based high-voltage direct-current (MMC-HVDC) system: (**a**) single line diagram; (**b**) circuit diagram; (**c**) AC side voltage.

As $n_{up} + n_{low} = 1$ and $n_{up}, n_{low} \epsilon \{0, 1 \ldots n\}$ based on Equation (1), $V_{C(a)}$ will change in discrete steps from $V_{dc}/2$ to $-V_{dc}/2$ with a step size of $\frac{V_{dc}}{n}$. By using the capacitor voltage balancing technique, the voltage of each cell is perfectly regulated at $\frac{V_{dc}}{n}$. The converter will generate an ideal $(n+1)$

level sinusoidal waveform for the AC side system with respect to the DC side midpoint as shown in Figure 1c [29]. In hardware implementation, the capacitor voltages of SMs are measured using large number of voltage sensors. It increases hardware complexity and also introduces errors in signal measurements, which affects the sinusoidal ideal voltage waveform [30].

The converter voltage ($V_{up,low}$) in phase a can be described as follows:

$$(V_{up,low}(a)) = \sum_{n=1}^{N} S_n V_c \tag{2}$$

where

$$S_n = \begin{cases} 1, \text{ if } n_{th}\text{cell is inserted} \\ 0, \text{ if } n_{th} \text{ cell is by passed} \end{cases}$$

The switching signal (s) finds the converter arm voltage based on $v_{up,low}^{ref}$ for the corresponding upper and lower arms. The dynamics of converter control include the grid side current (i_1), output converter voltage at the AC side (V_c), DC side current (I_{dc}), and internal circulating current (i_{circ}) [31]. Using Kirchhoff's voltage law in converter phase a, the following expressions are derived:

$$\frac{V_{dc}}{2} - V_{up(a)} - L\frac{di_{1u}}{dt} = V_g \tag{3}$$

$$-\frac{V_{dc}}{2} + V_{low(a)} + L\frac{di_{1l}}{dt} = V_g \tag{4}$$

Adding Equations (3) and (4), the dynamics of the converter output current at AC side is given as:

$$\frac{L}{2}\frac{di_1}{dt} = e_a - V_g \tag{5}$$

where $e_a = \frac{V_{up(a)} - V_{low(a)}}{2}$ is the inner generated voltage in phase a, V_g is the grid side voltage, i_{1u}, i_{1l} is the upper and lower arm currents, and L $(L = L_t + L_{arm}/2)$ is the equivalent inductance of the transformer and converter arm. The AC side current in phase a can be expressed as:

$$i_1 = i_{1u} - i_{1l} \tag{6}$$

The differential current i_{diff} of the convertercan be defined as the current flowing through each phase of the converter:

$$L_{arm}\frac{di_{\text{diff a}}}{dt} = \frac{V_{dc}}{2} - \frac{V_{up(a)} + V_{ow(a)}}{2} \tag{7}$$

where

$$i_{diffa} = \frac{i_{1u} + i_{1l}}{2} \tag{8}$$

The differential current from Equation (8) consists of two current components:

$$i_{diff} = \frac{i_{dc}}{3} + i_{cir} \tag{9}$$

The voltage to control the circulating current can be derived as:

$$v_{cir} = \mathrm{V_{dc}} - \frac{V_{up(a)} + V_{ow(a)}}{2} \tag{10}$$

The upper and lower currents in each arm are equal to half of the phase current i_1, one third of DCcurrent i_{dc}, and the circulating current i_{cir}.

$$i_{1u} = \frac{i_1}{2} + \frac{i_{dc}}{3} + i_{cir} \tag{11}$$

$$i_{1l} = -\frac{i_1}{2} + \frac{i_{dc}}{3} + i_{cir} \tag{12}$$

The currents (i_1) and (i_{cir}) are controlled through voltages $V^{\text{ref}}_{up(a)}$ and V^{ref}_{cir}, whereas converter SMs are inserted according to references ($V^{\text{ref}}_{up,low}$) during each time step.

3. MMC Control System

The MMC-HVDC control system comprises the following components:

1. System level (DC voltage control/active and reactive power);
2. Lower level control (circulating current control);
3. Capacitor voltage balancing control.

The system level control can be implemented using the direct or vector control strategy [32], as shown in Figure 2. This paper implements the vector current control strategy, which consists of a cascaded loop structure, i.e., an outer control loop (power/voltage) and an inner control loop (current). The outer loop feeds the current references for the inner current controllers. The current controller introduces decoupled control of reactive and active powers by controlling its q-axis and d-axis current components.

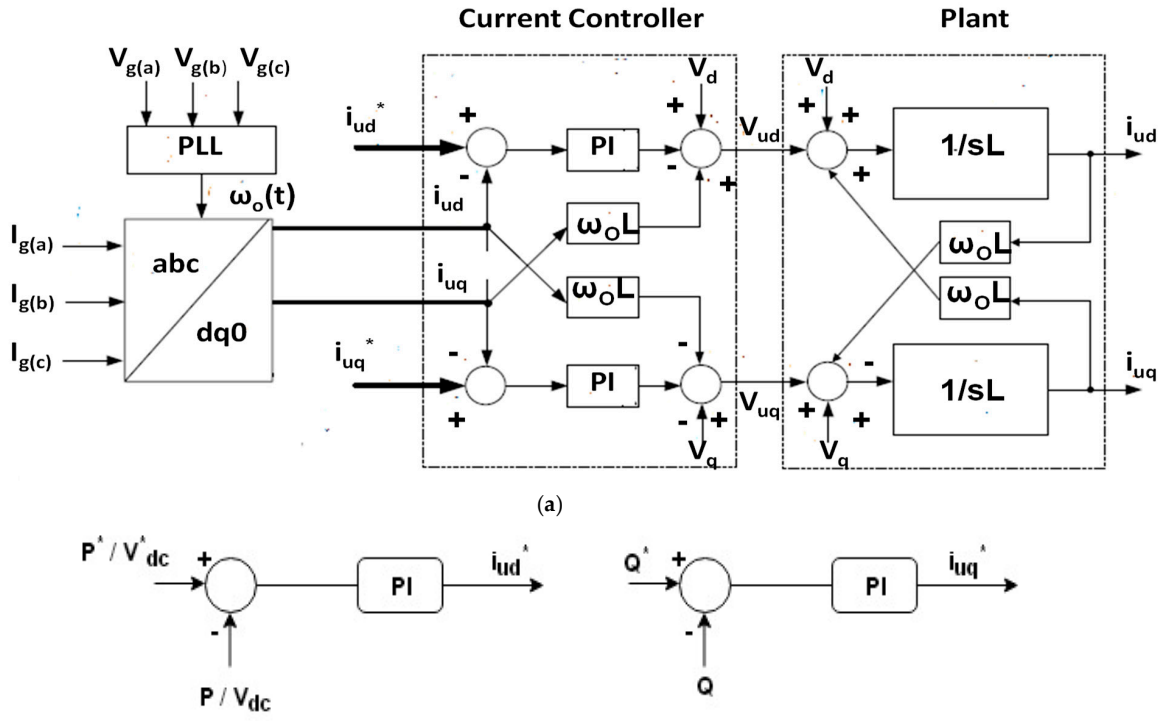

Figure 2. (**a**) Inner current control; (**b**) Outer loop power and voltage.

The circuit model of MMC (shown in Figure 1a) is connected to a symmetrical three-phase balanced grid with a frequency of ω_o. Its voltage and current equations are as follows:

$$\mathrm{V}_{\mathrm{g(a)}}(\mathrm{t}) = \sqrt{2}V sin(\omega_o t) \tag{13}$$

$$\mathrm{V}_{\mathrm{g(b)}}(\mathrm{t}) = \sqrt{2}V \sin\left(\omega_o t - \frac{2\pi}{3}\right) \tag{14}$$

$$\mathrm{V}_{\mathrm{g(c)}}(\mathrm{t}) = \sqrt{2}\,\mathrm{V}\ \sin\left(\omega_o \mathrm{t} + \frac{2\pi}{3}\right) \tag{15}$$

$$\mathrm{I}_{g(a)}(\mathrm{t}) = \sqrt{2}\,\mathrm{I}\,\sin(\omega_o \mathrm{t} - \varphi) \tag{16}$$

$$\mathrm{I}_{g(b)}(\mathrm{t}) = \sqrt{2}\,\mathrm{I}\,\sin\left(\omega_o \mathrm{t} - \frac{2\pi}{3} - \varphi\right) \tag{17}$$

$$\mathrm{I}_{g(c)}(\mathrm{t}) = \sqrt{2}\,\mathrm{I}\,\sin\left(\omega_o \mathrm{t} + \frac{2\pi}{3} - \varphi\right) \tag{18}$$

Each arm voltage can be regulated to get the required current. The output of each arm is half of the phase current.

$$L\frac{d}{dt}i_{1u}(t) = -V_{up(a)}(t) - V_{g(a)}(t) \tag{19}$$

$$L\frac{d}{dt}i_{1l}(t) = -V_{low(a)}(t) + V_{g(a)}(t) \tag{20}$$

The expression for the DC side current in the upper and lower arms in three leg is:

$$\frac{I_{dc}}{3} = i^{dc}_{1(u/l)}(t) = i^{dc}_{2(u/l)}(t) = i^{dc}_{3(u/l)}(t) \tag{21}$$

Three-phase AC current signals are transformed into DC signals, which is more appropriate for a control system design. The d-q current components in a rotating reference frame is based on the Park transformation as implemented in Equation (22) [33]. The desired d-q current quantities can be determined by the current magnitude and phase in a three-phase system.

$$\begin{bmatrix} \mathrm{i_{du}(t)} \\ \mathrm{i_{qu}(t)} \\ \mathrm{i_{ou}(t)} \end{bmatrix} = \frac{2}{3}\begin{bmatrix} \sin(\omega_o \mathrm{t}) + \sin\left(\omega_o \mathrm{t} - \frac{2\pi}{3}\right) + \sin\left(\omega_o \mathrm{t} + \frac{2\pi}{3}\right) \\ \cos(\omega_o \mathrm{t}) + \cos\left(\omega_o \mathrm{t} - \frac{2\pi}{3}\right) + \cos\left(\omega_o \mathrm{t} + \frac{2\pi}{3}\right) \\ \frac{1}{2}\,\frac{1}{2}\,\frac{1}{2} \end{bmatrix} . \begin{bmatrix} \mathrm{i_{g(a)}(t)} \\ \mathrm{i_{g(b)}(t)} \\ \mathrm{i_{(c)}(t)} \end{bmatrix} \tag{22}$$

By taking the derivative of Equations (19), (20) and (22), the equations in the d-q reference frame for the inner current dynamics are given as:

$$L\frac{d}{dt}i_{ud}(t) - \omega_o L i_{ud} = -V_{ud}(t) - V_d(t) \tag{23}$$

$$L\frac{d}{dt}i_{uq}(t) + \omega_o L i_{uq} = -V_{uq}(t) - V_q(t) \tag{24}$$

According to Equations (23) and (24), direct and quadrature current axes of terms $\omega_o L i_{ud}$ and $\omega_o L i_{uq}$ are coupled. De coupling of these terms can be achieved by using control inputs V_{ud} and V_{uq} as shown in Figure 2a. The V_{ud} and V_{uq} are the reference voltages used to generate insertion indices for each leg. The outer controllers compare reference values, active power, DC voltage, reactive power ($\mathrm{P^*, V^*dc, Q^*}$), and measured values ($\mathrm{P, V_{dc,}, Q}$) using PI controllers, as shown in Figure 2b.

The PI compensators are tuned based on the open loop approach [34]. The decoupled system is represented as a first order transfer function:

$$G_s = \frac{K}{1 + s\mathrm{T}} \tag{25}$$

The PI compensator can be shown as:

$$G_O = K_i . \frac{1 + sT_i}{sT_i} \tag{26}$$

where $K = \frac{1}{R}$ and $T = \frac{L}{R}$.

The open loop transfer functions of the current control loop can be shown as:

$$G_O = K_p\left(\frac{1+sT_i}{sT_i}\right)\left(\frac{K}{1+sT}\right) \tag{27}$$

The time constant T_i is selected as equal to the dominant time constant of the entire system, i.e., $T_i = T = \frac{L}{R}$, to achieve a phase margin of 60° in order to meet the stability criteria. The proportional gain of the controller is chosen as $K_P = \mathrm{L}/\tau$.

The independent control of active and reactive power based on vector current control can be expressed as:

$$P = \frac{3}{2}V_d i_d + V_q i_q \tag{28}$$

$$Q = \frac{3}{2}V_d i_d - V_q i_q \tag{29}$$

The q-axis component of voltage is set to zero, since phase locked loop (PLL) is synchronized to the grid voltage [35,36].

$$P = \frac{3}{2}V_d i_d \tag{30}$$

$$Q = -\frac{3}{2}V_d i_d \tag{31}$$

The circulating current is generated due to a mismatch between the output voltage of different phase arms and the DC voltage, and it is a negative-sequence (a-c-b) current and twice the fundamental frequency. Due to the circulating current, RMS arm current increases, which results in higher power losses [37]. The expression for inner differential current given in Equation (9) can be extended to three phases:

$$i_{diffa} = \frac{i_{dc}}{3} + i_{2f}\sin(2\omega_o t + \varphi_o) \tag{32}$$

$$i_{diffb} = \frac{i_{dc}}{3} + i_{2f}\sin\left[2(\omega_o t - \frac{2\pi}{3}) + \varphi_o)\right] \tag{33}$$

$$i_{diffc} = \frac{i_{dc}}{3} + i_{2f}\sin\left[2(\omega_o t + \frac{2\pi}{3}) + \varphi_o)\right] \tag{34}$$

where i_{2f} is the double frequency circulating current and φ_o is the phase angle. As evident from Equations (32) to (34), the DC current (component) is needed to keep the SM capacitor energy at the required level. However, higher order harmonics may be needed inside the circulating current to reduce the ripple effect of the SM capacitor.

The capacitor voltage balancing controller enables the energy variation in each sub-module to be shared equally (by each converter arm). The voltage of the SM should be kept approximately equal to its theoretical value V_{dc}/n (n is number of SMs in each arm), otherwise capacitor voltages will be unbalanced, and the AC output voltage will be difficult to control.

4. Average Model of MMC

The continuous model of MMC shown in Figure 1b can be developed by considering a cell's internal dynamics as an arm equivalent. Then, the converter arm can be modelled as variable capacitances, with their values determined by the insertion index n(t) i.e., n_u and n_l (upper and lower arm), which turns into a continuous parameter. The capacitor voltages in each arm can be considered as controlled voltage sources. By considering $V_c^{\Sigma}(t)$ asthe sum of capacitor voltages in one arm, the voltage inserted by the arm, V_c, is given by:

$$V_c^p = n(t)V_c^{\Sigma}(t) \tag{35}$$

where p denotes number of the arms. Due to the series connection of inserted capacitors (c^p) inside an arm and the flow of the charging current $i(t)$, the increase in the capacitor voltage in that arm is:

$$\frac{dV_c^{\Sigma}(t)}{dt} = \frac{i(t)}{c^p} \tag{36}$$

Using Equation (38), the dynamics of capacitor voltages in the upper and lower arms can be written as [38]:

$$\frac{dV_u^{\Sigma}(t)}{dt} = \frac{n_u i_{1u}}{c^{arm}} \tag{37}$$

$$\frac{dV_l^{\Sigma}(t)}{dt} = \frac{n_l i_{1l}}{c^{arm}} \tag{38}$$

where c^{arm} is the capacitance in each arm. The upper and lower arm currents as per Equations (11) and (12) can be derived as:

$$i_{1u} = \frac{c^{arm} dV_u^{\Sigma}(t)}{n_u\, dt} \tag{39}$$

$$i_{1l} = \frac{c^{arm} dV_l^{\Sigma}(t)}{n_l\, dt} \tag{40}$$

According to Figure 1b, by inserting resistance R (arm converter resistance), the output voltage in phase a can be shown as:

$$V_{c(a)} = \frac{V_{dc}}{2} - Ri_{1u} - L_{arm}\frac{di_{1u}}{dt} - n_u V_u^{\Sigma}(t) \tag{41}$$

$$V_{c(a)} = -\frac{V_{dc}}{2} + Ri_{1l} + L_{arm}\frac{di_{1l}}{dt} + n_l V_l^{\Sigma}(t) \tag{42}$$

Subtracting Equation (42) from (41) and using Equations (8), (37)–(40) gives the average model of one leg of an MMC in Equation (43):

$$\begin{bmatrix} i_{diff} \\ V_u^{\Sigma} \\ V_l^{\Sigma} \end{bmatrix} = \begin{bmatrix} -\frac{R}{L} & \frac{-n_u}{2} & \frac{-n_L}{2} \\ \frac{n_u}{c^{arm}} & 0 & 0 \\ \frac{n_L}{c^{arm}} & 0 & 0 \end{bmatrix} \begin{bmatrix} i_{diff} \\ V_u^{\Sigma} \\ V_l^{\Sigma} \end{bmatrix} + \begin{bmatrix} \frac{V_{dc}}{2} \\ \frac{n_u i_1}{2c^{arm}} \\ -\frac{n_l i_1}{2c^{arm}} \end{bmatrix} \tag{43}$$

This model will assume an even voltage distribution among the SMs in three legs of an MMC while the switching pattern is neglected.

5. Direct and Proposed Direct Modulation

Figure 3 shows as ingle phase equivalent circuit model based on an average model developed in Equation (43). The purpose of the modulation scheme is to provide insertion indices for all the arms of an MMC to achieve control system objectives. The insertion indices n_u and n_l determines the number of SMs inserted in each arm out of n number of SMs, having a continuous interval between 0–1. The inserted voltages can be varied between 0 and V_u^{Σ}.

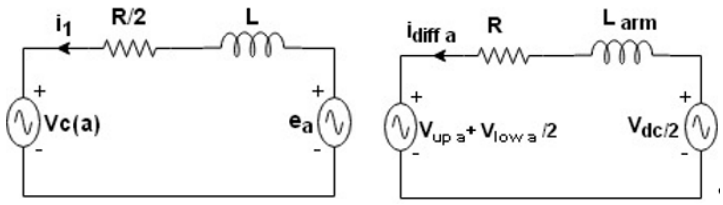

(**a**)AC side (**b**)DC side

Figure 3. Single phase equivalent circuit.

The direct modulation is based on the sinusoidal PWM generation; here, it is implemented with the vector current control method, which regulates inner-generated voltage e_a as given in Equation (5),

since it assumes an average capacitor voltage for all the SMs, but actually due to current flow capacitor voltage and its energy changes. The arm voltages are controlled by two complementary voltage references for upper and lower arms:

$$V_{upa\_ref} = \frac{V_{dc}}{2}[1 - m\cos(\omega_0 t)] - e_a \tag{44}$$

$$V_{lowa\_ref} = \frac{V_{dc}}{2}[1 + m\cos(\omega_o t)] - e_a \tag{45}$$

The term $m[m = \frac{I_1/2}{I_{dc}/2}]$ represents the modulation index (amplitude), and ω_o is angular frequency of the output voltage. If n is the number of utilized SMs in each arm, then voltage output has n + 1 level [39]. Since the duty ratio of the SMs in each arm is equal to its insertion index, voltage and capacitor currents are directly proportional to each arm insertion index. Since $V_c^{\sum}(t) = V_{dc}$, the circulating current is generated as per Equations (32) to (34). The circulating current is not controlled in the direct modulation approach. Traditionally, compensated modulation is used to control arm voltage oscillations generated in the direct modulation method. The insertion-index selection accounts for the capacitor voltage ripples, but its drawback is the delay in the measurement of the output current and DC link voltage [40,41].

The traditional approach of controlling the MMC-HVDC system consists of an AC side current control system and a separate circulating current suppression controller, which regulates unbalanced voltages inside each leg of a three-phase MMC converter. Both controllers operate in a cascade manner, which increases system complexity [42]. Unlike Reference [42], which set the inner differential current equal to zero in order to reduce capacitor voltage oscillations, a differential current controller is proposed in References [43,44], which regulates upper and lower arm capacitor energies in one phase of MMC.

In this paper, AC side current is controlled according to the active and reactive power references based on Equations (28) and (29). However, unlike Reference [45], which uses two separate PR controllers for controlling the AC side current and arm current of a converter during unbalanced voltage conditions, this paper proposes a new method of reducing the circulating current by the addition of 2nd and 4th harmonics in each arm current of an MMC, which reduces arm voltage oscillations due to reduction in excessive negative currents in a period. The waveform is shifted 120° and 240° for the other two legs. As upper and lower arm voltages have a constant DC voltage component in each leg during part of a period, the capacitor energy variations also reduce, thus the flow of circulating current decreases in each leg of a three-phase MMC.

The voltage references in the upper and lower arms are generated by a vector current control using Equations (23) and (24). By adding 2nd and 4th harmonics as per Equations (44) and (45), the voltage references for the proposed method can be expressed as:

$$V_{upa\_ref} = \frac{V_{dc}}{2}[1 - m\cos(\omega_o t)] - e_a + \frac{U_{2f}}{2}\sin(2\omega_o t + \varphi_o) + \frac{U_{4f}}{2}\sin(4\omega_o t + \varphi_o) \tag{46}$$

$$V_{lowa_{ref}} = \frac{V_{dc}}{2}[1 + m\cos(\omega_o t)] - e_a + \frac{U_{2f}}{2}\sin(2\omega_o t + \varphi_o) + \frac{U_{4f}}{2}\sin(4\omega_o t + \varphi_o) \tag{47}$$

The upper and lower arm currents using Equations (11), (12), (46), and (47) can be expressed in Equations (48) and (49). Less capacitor energy variations are obtained during the 120°degree part in a period compared to the sinusoidal arm current generated in the traditional direct modulation method, which is due to the constant nature of the DC current (analytical formulation results are shown in Appendix A).

$$i_{1u} = 1.5\left[\cos(\omega_o t) + \frac{20}{64}.\cos(2\omega_o t) + \frac{-0.5}{64}.\cos(4\omega_o t) + (1 + \frac{0.5}{64} + \frac{-20}{64})\right] \tag{48}$$

$$i_{1l} = 1.5\left[-\cos(\omega_o.t) + \frac{-20}{64}.\cos(2\omega_o t) + \frac{0.5}{64}.\cos(4\omega_o t) + (-1 + \frac{-0.5}{64} + \frac{20}{64})\right] \quad (49)$$

The converter output current in phase *a* using Equations (48) and (49):

$$i_l = i_{1u} - i_{1l}(t - \frac{T}{2}) \quad (50)$$

A flow chart to describe proposed direct modulation method is depicted in Figure 4.

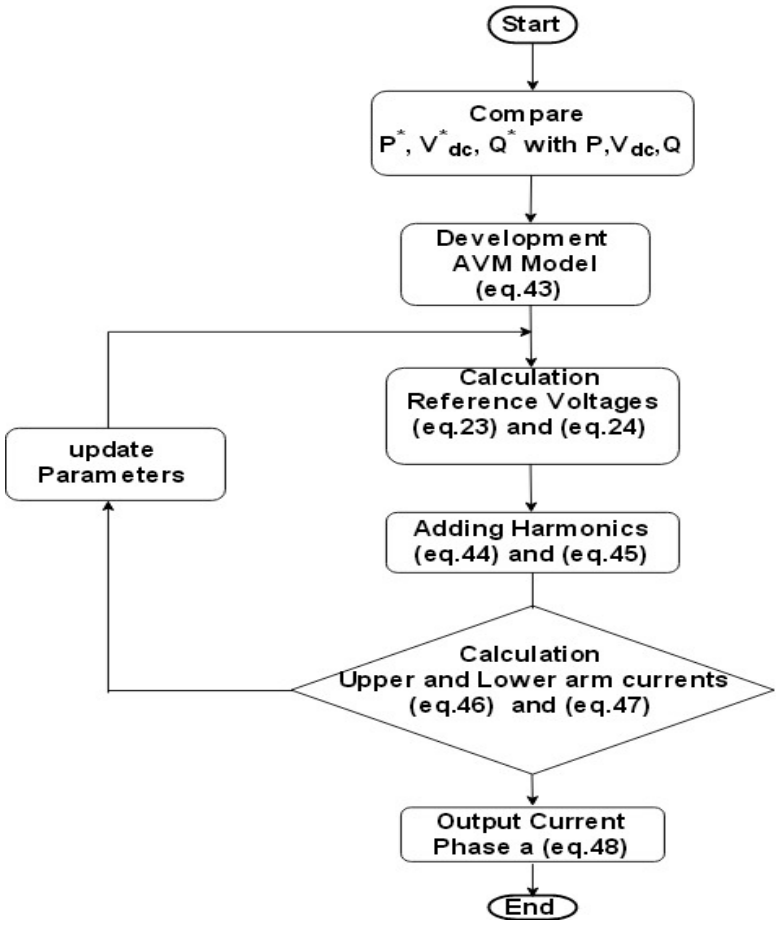

Figure 4. Flowchart of proposed direct modulation.

6. Analytical and Simulation Results

A two terminal symmetrical monopole MMC-HVDC shown in Figure 1 is simulated in PSCAD/EMTDC software. A master–slave approach is used, in which one power converter regulates the DC voltage and the other converter regulates the active power, whereas reactive power can be controlled independently at both sides of the AC side terminals. A vector current control is applied to the MMC here; the outer power controller and inner current controllers are similar to VSC (voltage source converter) traditional two-level configurations [46]. However, unlike the VSC two-level configuration, the circulating current is generated inside the MMC due to inner voltage differences among the phase units without influencing AC side voltages and currents [47]. The active and reactive powers are selected as control objectives similar to the VSC two-level configuration. Furthermore, the DC line is modelled using cascaded π-sections developed in [48].

A reference DC bus voltage of 640 kV with a power of 1000 MVA from terminal T_2 to terminal T_1 was considered. Both MMCs operate at s 0.96 power factor and generate 40 MVAr to meet the required

reactive power demand at the AC side of the HVDC system. The real and reactive current components i_{ud} and i_{uq} shown in Figure 2a adjusts the real and reactive power demand of the HVDC system.

Figure 5 shows simulation results of the MMC-HVDC system. Figure 5a–d shows the real powers (P_1, P_2), reactive powers (Q_1, Q_2), the DC bus voltage maintained at 640 kV, and the current in the HVDC line using direct and proposed direct modulation techniques.

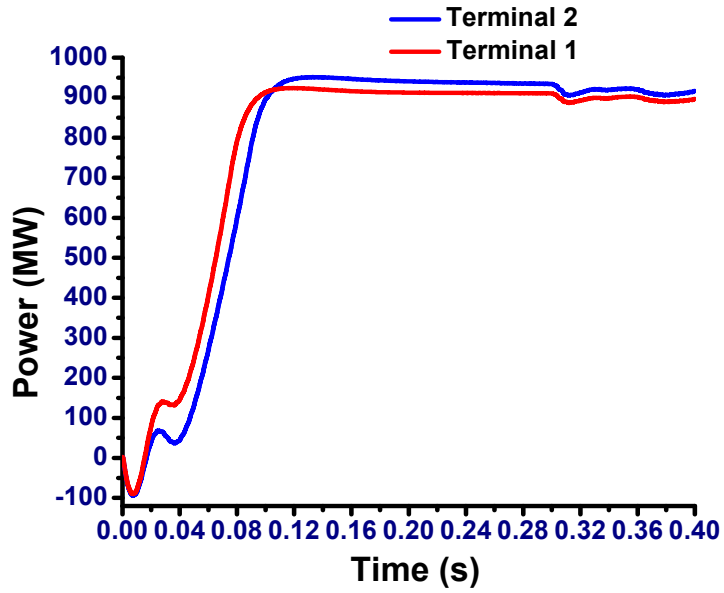

(**a**)

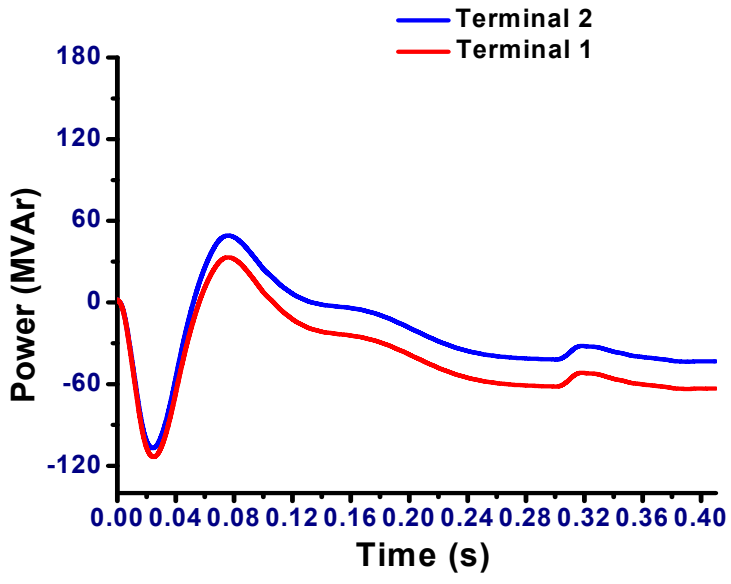

(**b**)

Figure 5. *Cont.*

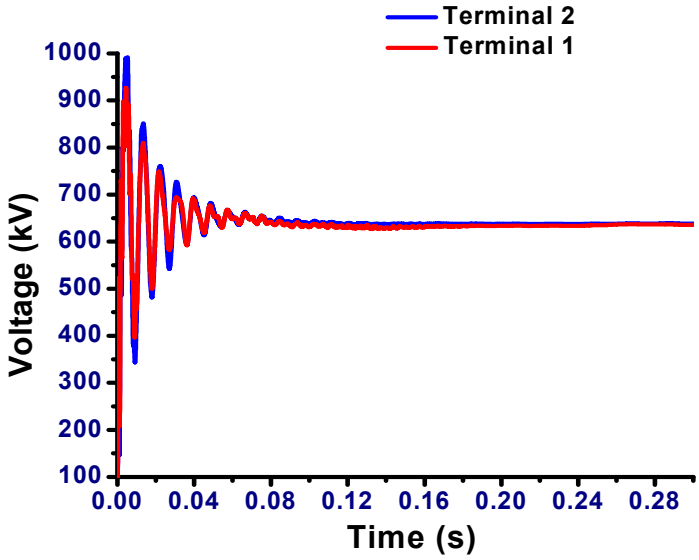

(**c**)

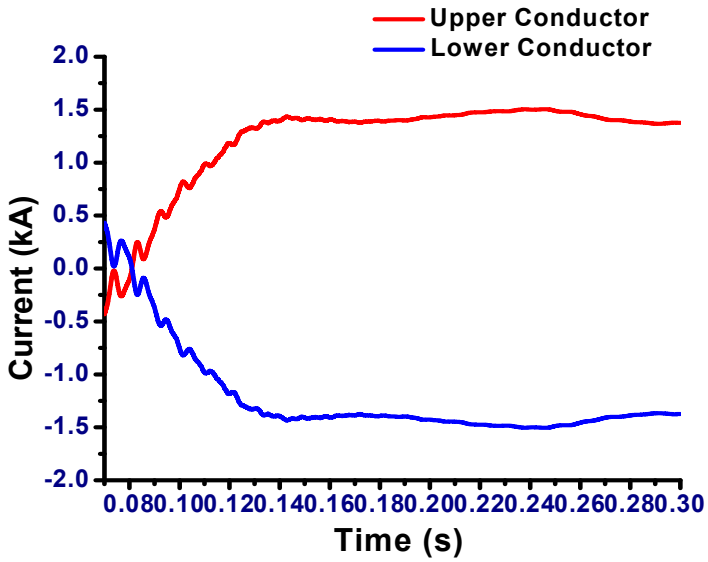

(**d**)

Figure 5. Results of (**a**) P_1, P_2 at T1and T2; (**b**) Q_1, Q_2 at T1and T2; (**c**) DC bus voltage at T1and T2; and (**d**) current in the DC line.

The system level control (active and reactive power) of MMC-HVDC at terminal T_2 and T_1 based on Equations (30) and (31) is shown in Figure 5a,b. At 0.08 s, the active power around both terminals are controlled to maintain their reference values (P = 960MW). The AC side reactive power is controlled at 40 MVAr at 0.1 s. From t = 0 to t =0.05 s, there is a small over-shoot in AC reactive power, but it quickly reaches a stable value at around 0.08 s.

At the rectifier side terminals T_2 and T_1, DC voltage is controlled at the reference value of 640 kV. Due to changes in active power at t = 0 s to t = 0.08 s, small transients are generated in DC voltages, which finally reaches the reference value at 0.08 s due to the DC voltage controller as shown in Figure 5c. The current in the upper and lower DC line is shown in Figure 5d. Due to small oscillations in DC power, there are small transients in the DC current, which finally reaches steady state at the reference value of around 1 kA at 0.14 s.

Figure 6a,b shows the three-phase line-to-line voltage and the three-phase current, representing the AC system connected to the MMC-HVDC system. The MMC grid side three-phase line-to-line output voltage and output current waveforms are shown in Figure 6c,d. The direct modulation and proposed direct modulation methods are tested on the MMC-HVDC system as shown in Figure 1a.

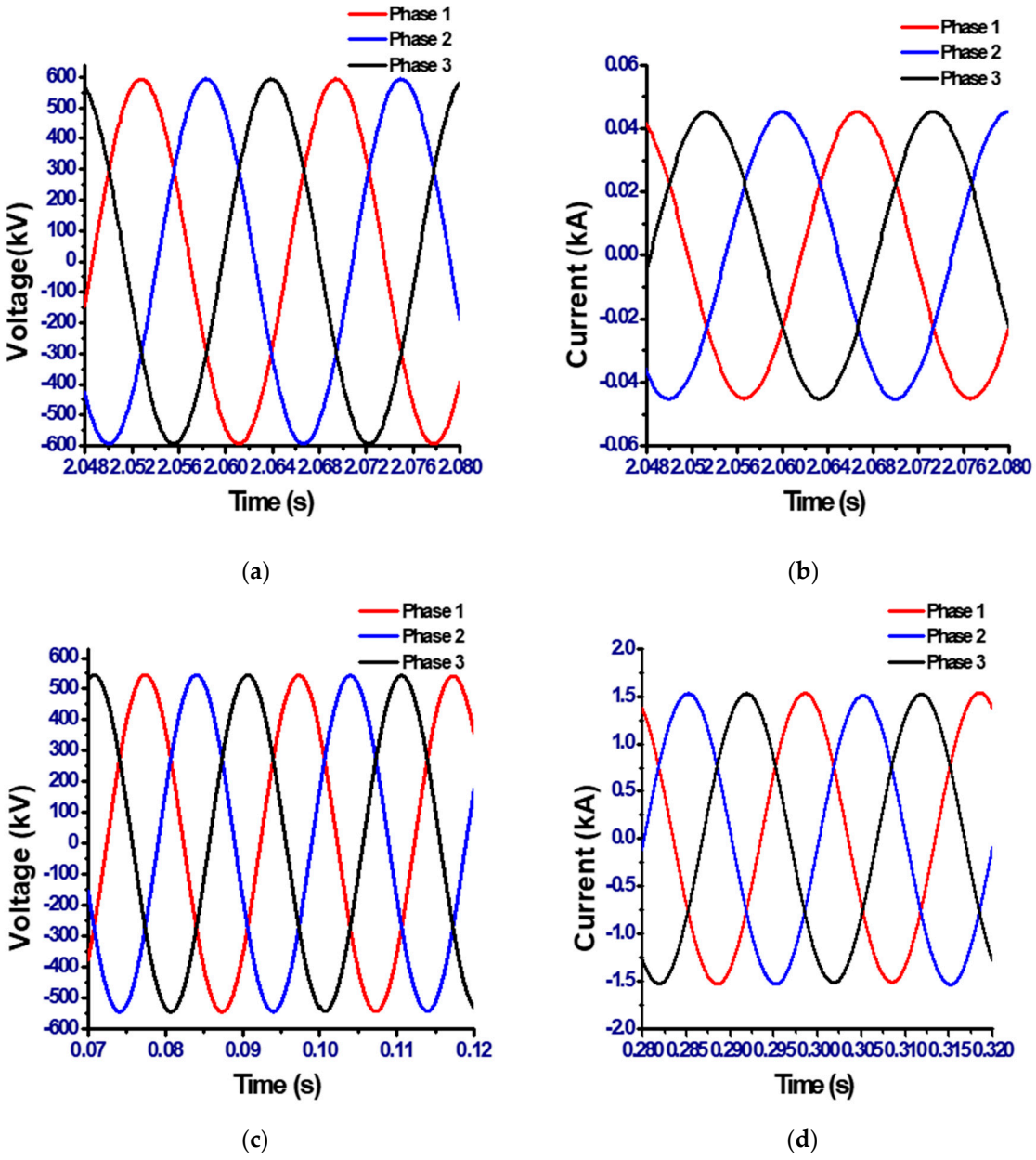

Figure 6. Results of (**a**) grid side voltage (peak line-to-line); (**b**) grid side current; (**c**) converter AC (peak line-to-line) side voltage; and (**d**) converter AC side current.

Figure 7a,b shows the voltage reference signals used to generate firing signals for SMs in each arm of MMC. The direct modulation and proposed method is implemented by vector current control method based on Equations (44)–(47). The upper and lower arm current waveforms using direct modulation and the proposed direct modulation can be observed in Figure 7c–f. These simulation results are based on the analytical Equations, derived in (11), (12), (39), (40), (48) and (49). Due to the flow of the circulating current, the upper and lower arm current peak values are distorted during the direct modulation approach.

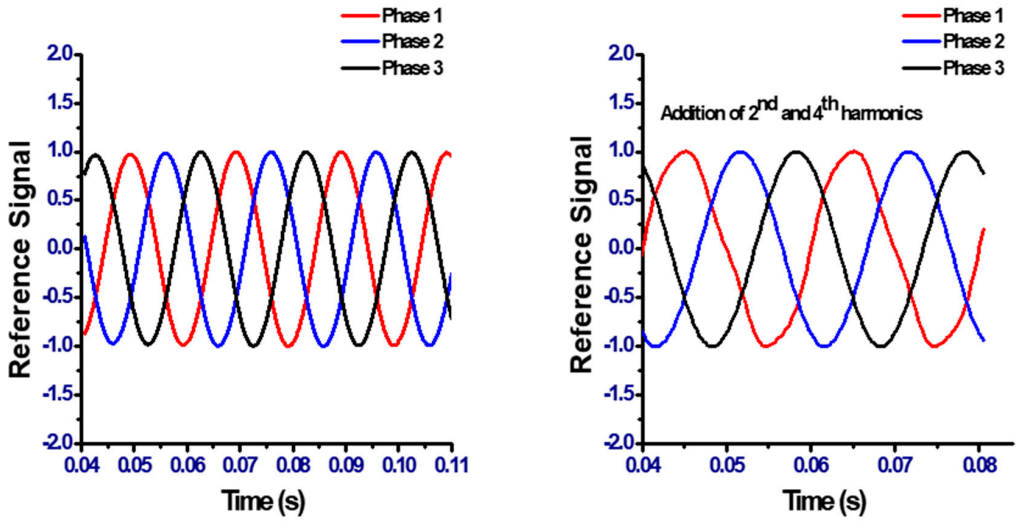

(**a**)

(**b**)

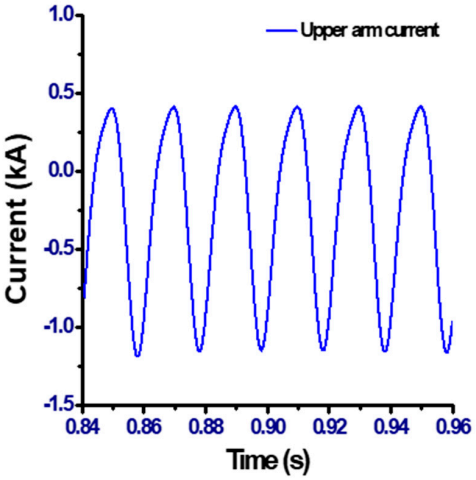

(**c**)

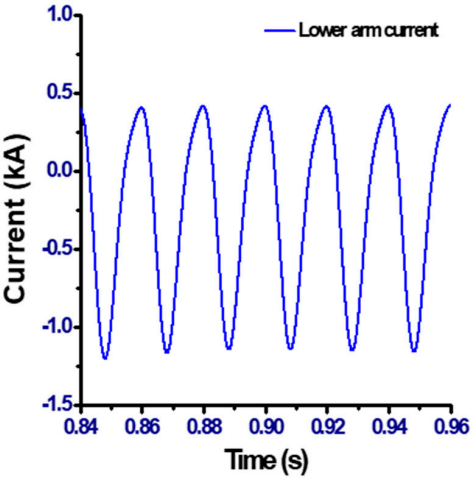

(**d**)

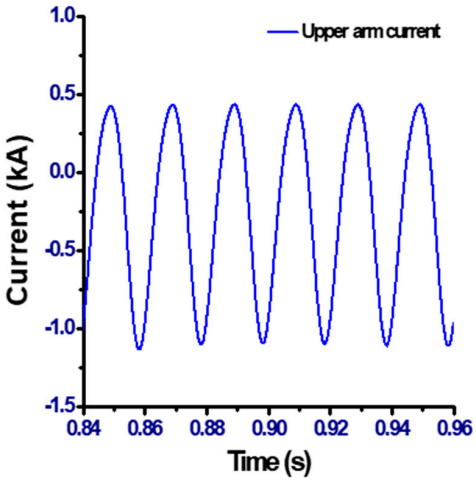

(**e**)

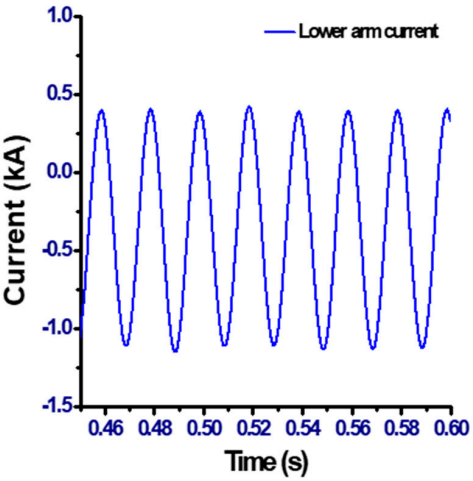

(**f**)

Figure 7. *Cont.*

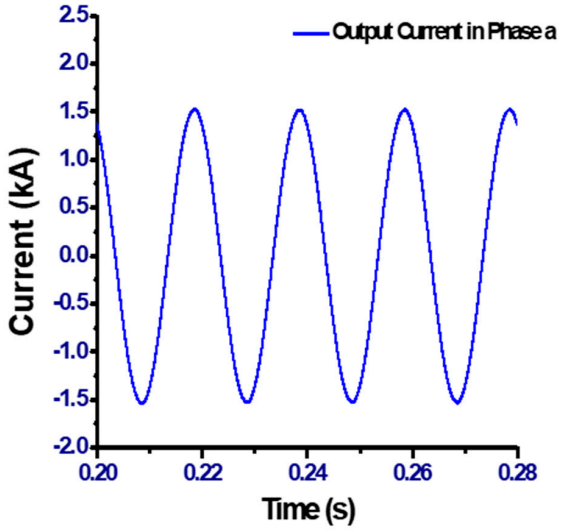

(**g**)

Figure 7. Results of (**a**) reference signal-direct modulation; (**b**) reference signal-proposed direct modulation; (**c**) upper arm current-direct modulation; (**d**) lower arm current-direct modulation; (**e**) upper arm current-proposed direct modulation; (**f**) lower arm current-proposed direct modulation; and (**g**) AC side current in phase *a*.

The distortion in the peak values of the arm currents during the proposed direct modulation method is removed due to a reduction in the circulating current without affecting the input and output current waveforms of the converter. The grid side output current waveform of the converter in phase *a* is shown in Figure 7g. The addition of even order harmonics does not influence the AC side output current of the converter.

Figure 8a,b shows the three-phase arm voltages for the direct modulation and proposed direct modulation methods. Due to the presence of the DC component at the top and bottom of arm voltages, there is a reduction in capacitor energy variations as DC voltage is constant (smooth) in a part of a period that reduces arm voltage oscillations in each leg of a three-phase MMC. The peak arm voltages (640 kV) in the proposed modulation method are lowered and flatter compared to peak arm voltages in the direct modulation method, which results in less oscillation.

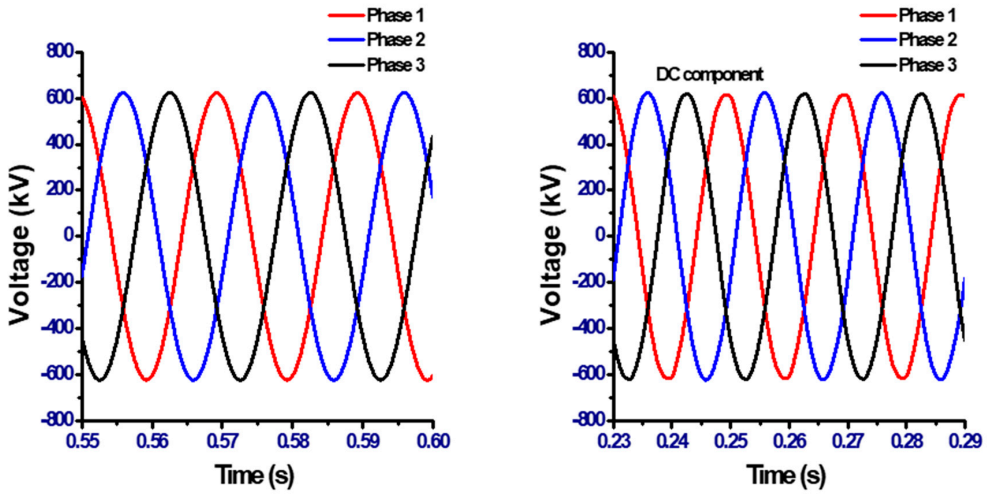

(**a**) (**b**)

Figure 8. Results of (**a**) arm voltages-direct modulation and (**b**) arm voltages-proposed direct modulation.

As per Equation (9), Figure 9a,b shows the i_{diff} currentin one leg. In Figure 8a, due to direct modulation, a circulating current is generated. In Figure 8b, due to a reduction in arm voltage oscillations by constant DC voltages, the circulating current amplitude is also reduced.

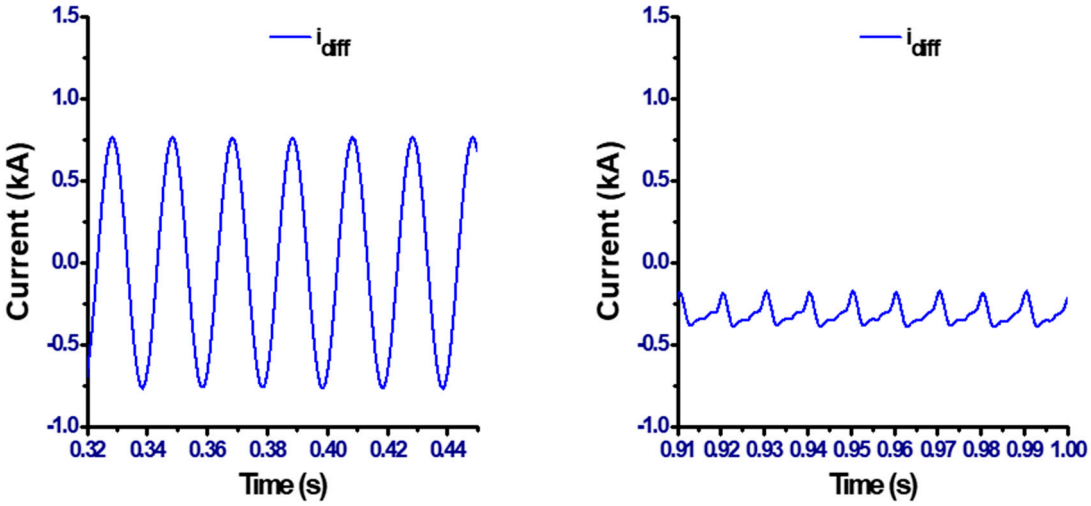

(**a**) (**b**)

Figure 9. Results of (**a**) circulating current-direct modulation and (**b**) circulating current-proposed direct modulation method.

A change in capacitor energy $W_{c(t)}$ over half a period using the traditional direct modulation method and the proposed method can be calculated using Equation (51) based on simulation results and parameters available in Table 2:

$$W_{c(t)} = \int_{-0.01}^{t} I_{leg(t)}.V_{leg(t)} \tag{51}$$

(a) Direct modulation

$$I_{leg(t)} = AC\ current + DC\ current$$

$$V_{leg(t)} = DC\ voltage - AC\ voltage$$

(b) Proposed method

$$I_{leg(t)} = AC\ current + A.cos(2.\omega.t) + B.cos(4.\omega.t) + DC\ current$$

$$V_{leg(t)} = DC\ voltage - AC\ voltage$$

where $I_{leg(t)}$ is the leg current and $V_{leg(t)}$ is the leg voltage. Less capacitor energy is witnessed during the proposed method compare to the direct modulation method for the same input and output power as shown in Figure 10a,b.

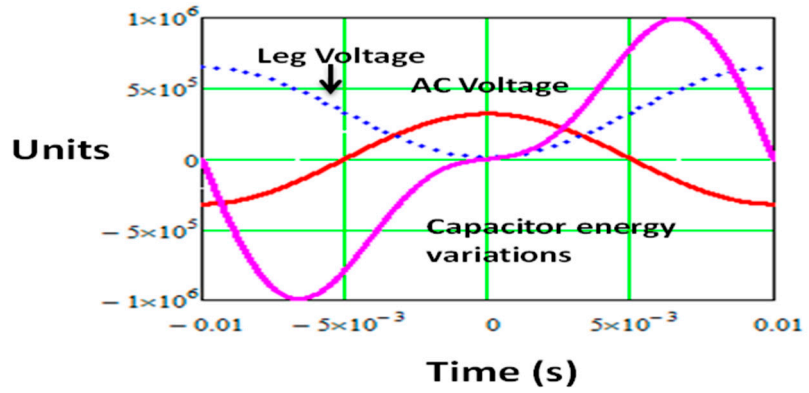

(**a**)

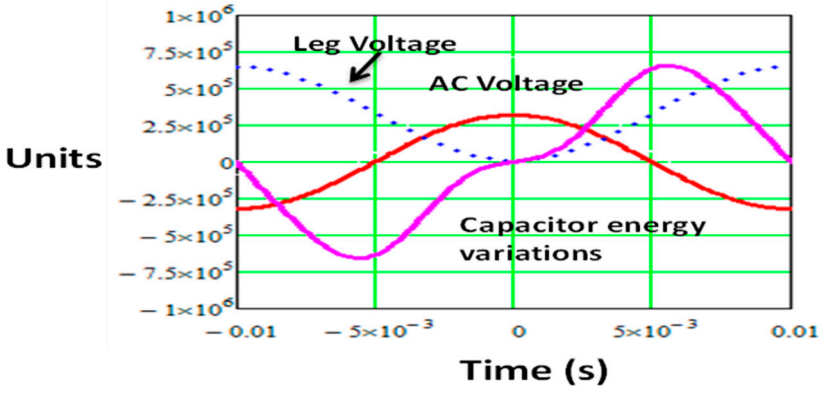

(**b**)

Figure 10. Results of (**a**) change in capacitor energy-direct modulation and (**b**) change in capacitor energy-proposed method.

Analytical and simulation results are compared in Table 1. Due to the proposed modulation, method RMS arm current is reduced compared to the direct modulation method, which is an important factor for power loss minimization in a three-phase MMC. The circulating current amplitude is also minimized due to the proposed method.

Table 1. Comparison of analytical and simulation results.

Quantity	Symbol	Direct Modulation		Proposed Direct Modulation	
		Amplitude	RMS Current	Amplitude	RMS Current
Upper Arm Current	i_{1u}	1.5 kA	0.75 kA	1.5 kA	0.65 kA
Lower Arm Current	i_{1l}	1.5 kA	0.75 kA	1.5 kA	0.65 kA
Output Current in Phase *a*	i_1	1.5 kA	-	1.5 kA	-
Differential Current	i_{diff}	1 kA	-	0.2 kA	-

The HVDC system parameters are given in Table 2.

Table 2. HVDC System Parameters.

Apparent Power (S)	1000 MVA
Active power (P)	960 MW
Grid side AC voltage	420 kV
Converter side AC voltage	380 kV
DC side voltage	$\pm$320 kV
DC side current	1.5 kA
Transformer connection	Y/Δ
Arm capacitor	28 μF
Arm inductance (continuous)	76 mH
Transformer inductance	15 mH
Arm resistance	0.8 Ω
DC Line (two conductors)	400 km
Ac side Power Factor $(Cos\varphi_L)$	0.96
Angular frequency	341 d/s

The advantages of proposed method can be summarized as follows:

- The AC component of the circulating current needs to be reshaped to reduce the voltage ripple in the capacitor; otherwise, it increases loss. Its DC current component is important to keep the capacitor voltages around a reference value.
- In the proposed method, the circulating current amplitude is reduced while keeping a balance between higher order harmonics and lower order harmonics inside the arm current.
- The RMS value of the arm current is also reduced compared to other techniques as clearly mentioned in the literature review.

7. Conclusions

A comprehensive analysis and modelling of the MMC-HVDC system using a non-linear average model based on the direct modulation scheme is carried out in this work. A vector current control strategy is implemented for all the discussed modulation methods. The direct modulation strategy does not control the circulating current in a MMC.

A new method is implemented for the reduction of circulating currents using a direct modulation approach. This strategy is based on the fact that the addition of even order harmonics leads to a decrease in arm voltage oscillations by restricting the flow of negative currents, while having smooth DC current components in each arm during part of a period without affecting input and output current waveforms. Less capacitor energy variations are obtained with the proposed method compared to the direct modulation method. The sum of these even harmonics does not contribute to the DC link current of the HVDC system. The analytical and simulation results show the reduction in circulating current amplitude and RMS values of the arm current by the proposed direct modulation method. The detailed analysis of the proposed method on capacitor voltage ripple reduction on MMCs using a detailed model will be addressed in future publications.

Author Contributions: Conceptualization and analytical wave forms (A.V.d.B.); Methodology, software implementation and writing-original draft (K.H.); review, editing and formal analysis (S.A.K.); supervision (Q.U.H.).

Funding: This research received no external funding.

Conflicts of Interest: The authors declare no conflict of interest.

Nomenclature

P	Number of phases
n	Number of sub modules per arm
IGBTs	Insulated Gate Bipolar Transistors
PI	Proportional Integral
PR	Proportional Resonant
RMS	Root Mean Square Value
C	Sub module capacitance
$\frac{V_{dc}}{2}$	Dc bus voltage per pole
V_{dc}	Dc bus voltage pole-to-pole
L_t	Transformer inductance
L_{arm}	Arm inductance
L	Equivalent transformer and arm inductance
R	Arm resistance
τ	Time constant of the closed-loop step response
V_u^{Σ}	Sum capacitor voltages in upper arm
V_l^{Σ}	Sum capacitor voltages in lower arm
V_c^{Σ}	Total capacitor voltage
n_u, n_l	Insertion indices upper and lower arm
$V_{C(a)}$	Converter output voltage in phase a
$V_{up\ (a)}$	Inserted voltages in phase a upper arm
$V_{low\ (a)}$	Inserted voltages in phase a lower arm
e_aI	Inner generated voltage in phase a
c^{arm}	Capacitance of series connected n cells
i_1	AC current in phase a
i_{cir}	Circulating current
I_{dc}	DCcurrent
$(V_{up,low}^{ref},)$	Reference for e_a
v_{cir}	Internal voltage (driving i_{cir})
v_{cir}^{ref}	Reference for v_{cir}
f	AC side system frequency
ω_o	Angular frequency
Vg	Grid voltage

Appendix A

The expression in Equations (48) and (49) are derived as:

$T = 1/f$

T (period) = 0.02

$\omega_o = 2\pi f$
$\omega t = \pi$

Due to direct modulation arm current is a sinusoidal wave form:

$$i = V_m\ Sin\omega t \tag{A1}$$

$$Acos(\omega t) + Bcos(2\omega t) + Ccos(4\omega t) + D \tag{A2}$$

where D is a constant adapted to become zero in the middle.

By taking the 2nd and 4th (1st, 3rd, and 5th derivatives are zero) derivatives of Equation (A2):

$$-Acos(\omega t) + B(-4)cos(2\omega t) - C(16)cos(4\omega t) + D \tag{A3}$$

$$A - cos(\omega t) + B(16)cos(2\omega t) - C(256)cos(4\omega t) + D \tag{A4}$$

The following co-efficient are derived from Equations (A3) and (A4):

$$[A = 1.5\ ,\ B = \frac{20}{64}\ , C = \frac{-0.5}{64}, D = 0]$$

The results of upper and lower arm currents based on analytical formulation using Equations (48) and (49) is displayed in Figures A1 and A2, which shows the reduction in the negative half current by adding even order harmonics. Due to the presence of the DC current component, the arm voltage oscillations were also reduced. There are less capacitor energy variations, as DC voltage is constant during part of a period, which reduces the circulating current. The peak value of arm currents also reduces as negative arm current is more flat at the bottom. The DC current component in each arm will be the result of the DC input and output voltage. More input voltage less DC current based on Equation (50) is shown in Figure A3, which is almost similar to a sinusoidal arm current generation.

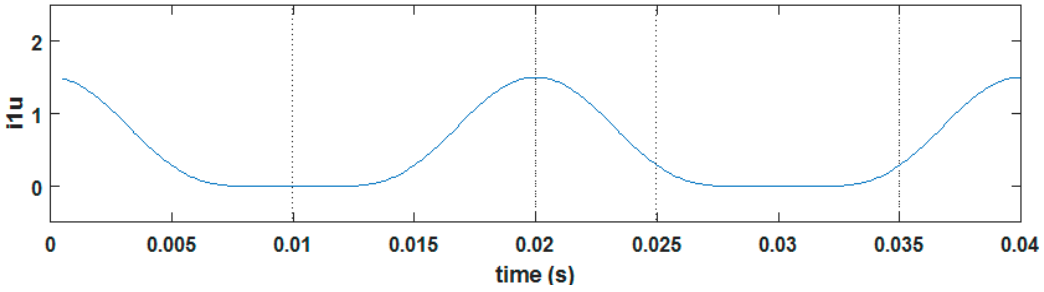

Figure A1. Upper arm current—proposed direct modulation.

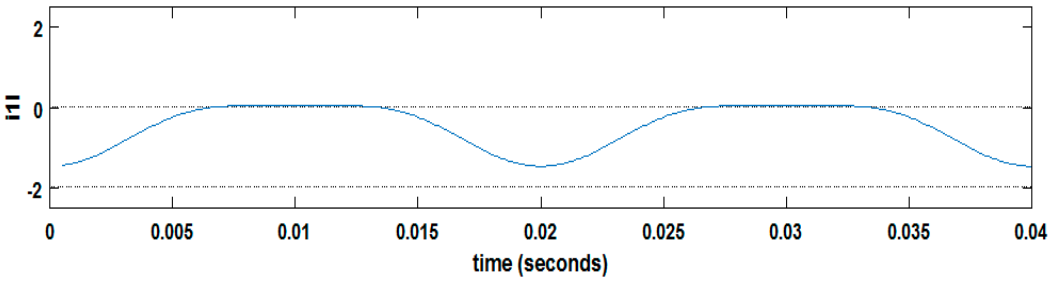

Figure A2. Lower arm current—proposed direct modulation.

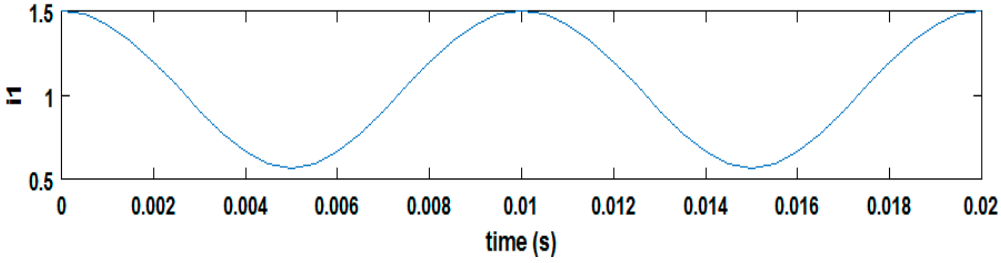

Figure A3. Leg current—proposed method.

References

1. Adam, G.P.; Finney, S.J.; Ahmed, K.H.; Williams, B.W. Modular multilevel converter modeling for power system studies. Presented at 4th International Conference on Power Engineering, Energy and Electrical Drives, Istanbul, Turkey, 13–17 May 2013.
2. Perez, M.A.; Bernet, S.; Rodriguez, J.; Kouro, S.; Lizana, R. Circuit Topologies, Modeling, Control Schemes, and Applications of Modular Multilevel Converters. *IEEE Trans. Power Electr.* **2015**, *30*, 4–17. [CrossRef]
3. Chaudhuri, N.R.; Oliveira, R.; Yazdani, A. Modeling and Stability Analysis of Modular Multilevel HVDC Converters. In Proceedings of the IEEE Power and Energy Society General Meeting, Denver, CO, USA, 26–30 July 2015.

4. Manitoba HVDC Research Center PSCAD. EMTDC 4.1 User's Manual. Available online: https://hvdc.ca/uploads/knowledge_base/pscad_manual_v4_6.pdf?t=1528395602 (accessed on 4 March 2019).
5. Saad, H.; Dennetiere, S.; Mahseredjian, J.; Delarue, P.; Guillaud, X.; Peralta, J.; Nguefeu, S. Modular Multilevel Converter Models for Electromagnetic Transients. *IEEE Trans. Power Deliver.* **2014**, *29*, 1481–1489. [CrossRef]
6. Teeuwsen, S.P. Simplified dynamic model of a voltage-sourced converter with modular multilevel converter design. In Proceedings of the IEEE/PES, Power System, Seatle, WA, USA, 15–18 March 2009; pp. 1–6.
7. Peralta, J.; Saad, H.; Dennetiere, S.; Mahseredjian, J.; Nguefeu, S. Detailed and averaged models for a 401-level MMC/HVDC system. *IEEE Trans. Power Deliver.* **2012**, *27*, 1501–1508. [CrossRef]
8. Krein, P.T.; Bentsman, J.; Bass, R.M.; Lesieutre, B.L. On the use of averaging for the analysis of power electronic systems. *IEEE Trans. Power Electr.* **1990**, *5*, 182–190. [CrossRef]
9. Peralta, J.; Saad, H.; Dennetiere, S.; Mahseredjian, J. Dynamic performance of averaged-value models for multi-terminal VSC-HVDC systems. In Proceedings of the IEEE Power and Energy Society General Meeting, San Diego, CA, USA, 22–26 July 2012; pp. 1–8.
10. Cigre, W.G. B4-57 Guide for the Development of Models for HVDC Converters in a HVDC Grid. Technical Brochures. Pairs, France, 2014. Available online: https://e-cigre.org/publication/604-guide-for-the-development-of-models-for-hvdc-converters-in-a-hvdc-grid (accessed on 3 March 2019).
11. Khan, S.; Tedeschi, T. Modeling of MMCfor Fast and Accurate Simulation of Electromagnetic Transients: A Review. *Energies* **2017**, *10*, 1161. [CrossRef]
12. Martinez-Rodrigo, F.; Ramirez, D.; Rey-Boue, A. Modular Multilevel Converters: Control and Applications. *Energies* **2017**, *10*, 1709. [CrossRef]
13. Rohner, S.; Weber, J.; Bernet, S. Continuous model of Modular Multilevel Converter with experimental verification. In Proceedings of the 2011 IEEE Energy Conversion Congress and Exposition, Phoenix, AZ, USA, 17–22 September 2011; pp. 4021–4028.
14. Chaudhuri, N.R.; Oliveira, R.; Yazdani, Y. Stability Analysis of Vector-Controlled Modular Multilevel Converters in Linear Time Periodic Framework. *IEEE Trans. Power Electr.* **2016**, *31*, 5255–5269. [CrossRef]
15. Ilves, K.; Antonopoulos, A.; Norrga, S.; Nee, H.P. Steady-State Analysis of Interaction between Harmonic Components of Arm and Line Quantities of Modular Multilevel Converters. *IEEE Trans. Power Electr.* **2012**, *27*, 57–68.
16. Antonopoulos, A.; Angquist, L.; Nee, H.P. On dynamics and voltage control of the modular multilevel converter. In Proceedings of the 13th European Conference on Power Electronics and Applications, Barcelona, Spain, September 2009; pp. 1–10.
17. Song, Q.; Liu, W.; Li, X.; Rao, H.; Xu, S.; Li, L. A Steady-State Analysis Method for a Modular Multilevel Converter. *IEEE Trans. Power Electr.* **2013**, *28*, 3702–3713. [CrossRef]
18. Vasiladiotis, M.; Cherix, N.; Rufer, A. Accurate Capacitor Voltage Ripple Estimation and Current Control Considerations for Grid-Connected Modular Multilevel Converters. *IEEE Trans. Power Electr.* **2014**, *29*, 4568–4579. [CrossRef]
19. Qin, J.; Saeedifard, M. Predictive control of a modular multilevel converter for a back-to-back HVDC system. *IEEE Trans. Power Del.* **2012**, *27*, 1538–1547.
20. Li, S.; Wang, X.; Yao, Z.; Li, T.; Peng, Z. Circulating current suppressing strategy for MMC-HVDC based on nonideal proportional resonant controllers under unbalanced grid conditions. *IEEE Trans. Power Electr.* **2015**, *30*, 387–397. [CrossRef]
21. Darus, R.; Pou, J.; Konstantinou, G.; Ceballos, S.; Agelidis, V. Circulating current control and evaluation of carrier dispositions in modular multilevel converters. In Proceedings of the IEEE ECCE Asia Downunder, Melbourne, VIC, Australia, 3–6 June 2013; pp. 332–338.
22. Zhang, M.; Huang, L.; Yao, W.; Lu, Z. Circulating harmonic current elimination of a CPS-PWM-based modular multilevel converter with a plug-in repetitive controller. *IEEE Trans. Power Electr.* **2014**, *29*, 2083–2097. [CrossRef]
23. Liang, Y.; Liu, J.; Zhang, T.; Yang, Q. Arm currentcontrol strategyfor MMC-HVDCunderUnbalancedConditions. *IEEE Trans. Power Deliver.* **2017**, *32*, 125–134. [CrossRef]
24. Engel, S.; De Doncker, R. Control of the modular multi-level converter for minimized cell capacitance. In Proceedings of the 14th European Conference on Power Electronics and Applications, Brimingham, UK, 30 August–1 September 2011; pp. 1–10.

25. Picas, R.; Pou, J.; Ceballos, S.; Zaragoza, J.; Konstantinou, G.; Agelidis, V. Optimal injection of harmonics in circulating currents of modular multilevel converters for capacitor voltage ripple minimization. In Proceedings of the IEEE ECCE Asia Downunder, Melbourne, VIC, Australia, 3–6 June 2013; pp. 318–324.
26. Wang, J.; Han, X.; Ma, H.; Bai, Z. Analysis and Injection Control of Circulating Current for Modular Multilevel Converters. *IEEE Trans. Ind. Electr.* **2019**, *66*, 2280–2290. [CrossRef]
27. Bergna-Diaz, G.; Suul, J.A.; D'Arco, S. Energy-based state-space representation of modular multilevel converters with a constant equilibrium point in steady-state operation. *IEEE Trans. Power Electr.* **2018**, *33*, 4832–4851. [CrossRef]
28. Hagiwara, M.; Akagi, H. PWMcontrol and experiment of modular multilevel converters. In Proceedings of the IEEE Power Electronics Specialists Conference, Rhodes, Greece, 15–19 June 2008; pp. 154–161.
29. Dekka, A.; Wu, B.; Zargari, N.R.; Fuentes, N.R. Dynamic Voltage Balancing Algorithm for Modular Multilevel Converter: A Unique Solution. *IEEE Trans. Power Electr.* **2016**, *31*, 952–963. [CrossRef]
30. Debnath, S.; Qin, J.; Bahrani, J.; Saeedifard, M.; Barbosa, P. Operation, Control, and Applications of the Modular Multilevel Converter: A Review. *IEEE Trans. Power Electr.* **2015**, *30*, 37–53. [CrossRef]
31. Ängquist, L.; Antonopoulos, A.; Siemaszko, D.; Ilves, K.; Vasiladiotis, M.; Nee, H.P. Open-loop control of modular multilevel converters using estimation of stored energy. *IEEE Trans. Ind. Appl.* **2011**, *47*, 2516–2524. [CrossRef]
32. Sood, V.; Patel, H. Comparison between direct and vector control strategy for VSC-HVDC system in EMTP-RV. In Proceedings of the 2010 Joint International Conference on Power Electronics, Drives and Energy Systems and 2010 Power India, New Delhi, India, 20–23 December 2010; pp. 1–6.
33. Egea-Alvarez, A.; Junyent-Ferré, A.; Gomis-Bellmunt, O. Active and reactive power control of grid connected distributed generation systems. In *Modeling and Control of Sustainable Power Systems*; Springer: Berlin, Germany, 2012; pp. 47–81.
34. Bahrani, B.; Kenzelmann, S.; Rufer, A. Multivariable-PI-based dq current control of voltage source converters with superior axis decoupling capability. *IEEE Trans. Ind. Electr.* **2011**, *58*, 3016–3026. [CrossRef]
35. Geddada, N.; Ukil, A.; Yeap, Y.M. Circulating Current Controller in dq Reference Frame for MMC Based HVDC System. In Proceedings of the 42nd Annual Conference, Industrial Electronics Society, IECON, Florence, Italy, 24–27 October 2016; pp. 3288–3293.
36. Zadeh, M.K.; Amin, M.; Suul, J.A.; Molinas, M.; Fosso, O.B. Small Signal Stability Study of the Cigré DC Grid Test System with Analysis of Participation Factors and Parameter Sensitivity of Oscillatory Modes. In Proceedings of the IEEE, Wroclaw, Poland, 18–22 August 2014; pp. 18–22.
37. Moranchel, M.; Bueno, E.; Sanz, I.; Rodríguez, F.J. New Approaches to Circulating Current Controllers for Modular Multilevel Converters. *Energies* **2017**, *10*, 86. [CrossRef]
38. Ahmed, N.; Angquist, L.; Norrga, S.; Antonopoulos, A.; Harnefors, L.; Nee, H.P. A Computationally efficient continuous model for the modular multilevel converter. *IEEE J. Em. Sel. Top. Power Electr.* **2014**, *2*, 1139–1148. [CrossRef]
39. Escalante, M.F.; Vannier, J.C. Direct approach for balancing the capacitor voltages of a 5-level flying capacitor converter. In Proceedings of the European Power Electronics Conference (EPE), Lausanne, Switzerland, 7–9 September 1999.
40. Harnefors, L.; Antonopoulos, A.; Norrga, S.; Angquist, L.; Nee, H.P. Dynamic analysis of modular multilevel converters. *IEEE Trans. Ind. Electr.* **2013**, *60*, 2526–2537. [CrossRef]
41. Harnefors, L.; Antonopoulos, A.; Ilves, K.; Nee, H.P. Global asymptotic stability of current-controlled modular multilevel converters. *IEEE Trans. Power Electr.* **2015**, *30*, 249–258. [CrossRef]
42. Tu, Q.; Xu, Z.; Xu, L. Reduced switching-frequency modulation and circulating current suppression for modular multilevel converters. *IEEE Trans. Power Deliver.* **2011**, *26*, 2009–2017.
43. Bergna, G.; Berne, E.; Egrot, P.; Lefranc, P.; Amir, A.; Vannier, J.; Molinas, M. An energy-based controller for hvdc modular multilevel converter in decoupled double synchronous reference frame for voltage oscillations reduction. *IEEE Trans. Ind. Electr.* **2013**, *60*, 2360–2371. [CrossRef]
44. Bergna, G.; Berne, E.; Lefranc, P.; Molinas, M. Modular multilevel converter-energy difference controller in rotating reference frame. In Proceedings of the 15th International Power Electronics and Motion Contorol Conference (EPE/PEMC), Novi Sad, Serbia, 4–6 September 2012; pp. 299–307.

45. Moon, J.W.; Park, J.W.; Kang, D.W.; Kim, J.M. A control method of HVDC-modular multilevel converter based on arm current under the unbalanced voltage condition. *IEEE Trans. Power Deliver.* **2015**, *30*, 529–536. [CrossRef]
46. Mohammadi, F. Power Management Strategy in Multi-Terminal VSC-HVDC System. In Proceedings of the 4th International Conference on Applied Research in Electrical, Mechanical Computer and IT Engineering, 4 October 2018.
47. Tu, Q.; Xu, Z.; Huang, H.; Zhang, J. Parameter design principle of the arm inductor in modular multilevel converter based HVDC. In Proceedings of the International Conference on Power System Technology, Hangzhou, China, 24–28 October 2010; pp. 1–6.
48. Rosendo Macias, J.; Gomez Exposito, A.; Bachiller Soler, A. A comparison of techniques for state-space transient analysis of transmission lines. *IEEE Trans. Power Deliver.* **2005**, *20*, 894–903. [CrossRef]